Development of a finite element musculoskeletal model with the ability to predict contractions of three-dimensional muscles

Junyan Li[1]*, Yongtao Lu[2]*, Stuart Miller[3], Zhongmin Jin[4], Xijin Hua[5]

Institute:

[1]School of Science and Technology, Middlesex University, London, UK

[2]Department of Engineering Mechanics, Dalian University of Technology, Dalian, China

[3]Sports and Exercise Medicine, Queen Mary University London, Mile End Hospital, London, UK

[4]School of Mechanical Engineering, Southwest Jiaotong University, Chengdu, China

[5]Institute for Biomechanics, ETH Zurich, Zurich, Switzerland

Key words: 3D finite element muscle model; musculoskeletal model; optimization of muscle contraction; knee biomechanics; gait

Corresponding author:

Junyan Li

ljyjerry@gmail.com

School of Science and Technology, Middlesex University, London, United Kingdom NW4 4BT

Yongtao Lu

yongtaolu@dlut.edu.cn

Department of Engineering Mechanics, Dalian University of Technology, Dalian, China

Abstract

Representation of realistic muscle geometries is needed for systematic biomechanical simulation of musculoskeletal systems. Most of the previous musculoskeletal models are based on multibody dynamics simulation with muscles simplified as one-dimensional (1D) line-segments without accounting for the large muscle attachment areas, spatial fibre alignment within muscles and contact and wrapping between muscles and surrounding tissues. In previous musculoskeletal models with three-dimensional (3D) muscles, contractions of muscles were among the inputs rather than calculated, which hampers the predictive capability of these models. To address these issues, a finite element musculoskeletal model with the ability to predict contractions of 3D muscles was developed. Muscles with realistic 3D geometry, spatial muscle fibre alignment and muscle-muscle and muscle-bone interactions were accounted for. Active contractile stresses of the 3D muscles were determined through an efficient optimization approach based on the measured kinematics of the lower extremity and ground force during gait. This model also provided stresses and strains of muscles and contact mechanics of the muscle-muscle and muscle-bone interactions. The total contact force of the knee predicted by the model corresponded well to the *in vivo* measurement. Contact and wrapping between muscles and surrounding tissues were evident, demonstrating the need to consider 3D contact models of muscles. This modelling framework serves as the methodological basis for developing musculoskeletal modelling systems in finite element method incorporating 3D deformable contact models of muscles, joints, ligaments and bones.

Introduction

Biomechanics plays an important role in the function of muscles, bones and joints. Computer modelling of the musculoskeletal system is by far the only non-invasive approach to predict biomechanics of joints and deep muscles. Most of the previous musculoskeletal models are based on multibody dynamics simulation, incorporating three-dimensional (3D) rigid bones attached by one-dimensional (1D) line-segment muscles. Additionally, 3D contact joints have been calculated within several recent models (Adouni et al., 2012, Chen et al., 2015). Although the models with 1D muscles are efficient to solve the redundancy issue, i.e. muscles outnumber equations of equilibrium requiring optimization to determine a unique solution of muscle forces, they have limited accuracy. This is because aspects including large muscle attachment areas, spatial fibre alignment within muscles, and contact and wrapping between muscles and surrounding tissues play important roles in the mechanics of musculoskeletal models and cannot be represented in 1D models (Webb et al., 2014). Importantly, 1D models do not provide biomechanical parameters such as stresses and strains of muscles and contact mechanics between muscles and surrounding tissues that are important for investigation of the function and degeneration mechanism of musculoskeletal systems. As such, more detailed models are required that incorporate 3D muscle representation.

By coupling boundary conditions between a rigid musculoskeletal model and a deformable knee model, predictions of deformation and contact mechanics in the knee were enabled (Halloran et al., 2010, Shu et al., 2018). However, this approach is not suitable for 3D muscles, because boundary conditions of 1D and 3D muscle models cannot be realistically coupled. Musculoskeletal models incorporating 3D muscles have been developed in finite element method, accounting for spatial fibre orientation and interactions between muscles and bones (Webb et al., 2014, Zöllner et al., 2015, Mo et al., 2018). However, the redundancy issue of muscle contractions has not been addressed in the previous 3D muscle models, which hampers the predictive capability of these models.

In order to address the above issues, the aim of this study was to develop a finite element musculoskeletal model with the ability to predict contractions of 3D muscles. Muscles with realistic 3D geometry, spatial muscle fibre alignment and muscle-muscle and muscle-bone interactions were accounted for. The redundancy issue of muscle contractions was solved through an efficient optimization approach. Additionally, the total contact force of the knee predicted by the model was compared to *in vivo* measurement data for validation.

Methods

The 3D geometric models of muscles and bones used in this study are based on the TLEM 2.0 database (Carbone et al., 2015). The model includes bones of the right lower extremity i.e. pelvis, femur, patella, tibia/fibula, talus and foot, connected by the hip, knee and ankle (**Fig. 1**). Only the principal muscles involved in flexion and extension of the knee including quadriceps (i.e. rectus femoris, vastus lateralis, vastus

intermedius and vastus medialis) and hamstrings (i.e. semitendinosus, semimembranosus, biceps femoris caput breve and biceps femoris caput longum) were incorporated in the model to enhance computational efficiency. The regions of tendon and muscle tissues were identified and some missing tendons connecting the muscles and bones were recreated in Solidworks (V2017, Dassault Systèmes, France) using a combination of MRI images, muscle geometry, bone landmarks and knowledge of anatomy (Drake et al., 2009).

The mesh was created in Hypermesh (V2017, Altair, USA), with the bones and muscles represented using 36162 four-noded tetrahedral elements and 18028 eight-noded hexahedral elements, respectively. The mesh density was selected such that a change of less than 5% difference in muscle forces occurred if the number of elements were doubled. The insertion/origin sites of the muscle/tendon tissues were rigidly attached onto the bones. Frictionless contact was defined for the muscle-muscle and muscle-bone interactions. Computational efficiency was enhanced by assuming the knee as a one degree-of-freedom hinge joint (flexion/extension) with the patella immobilized onto the tibia (Li et al., 2015), ankle and hip as three degrees-of-freedom ball-and-socket joints and bones as rigid.

Muscles and tendons were defined as incompressible transversely isotropic Mooney-Rivlin material incorporating muscle fibres that align along the geometry of muscles (**Fig. 1**) (Weiss et al., 1996). This constitutive model was described in detail in the FEBio Theory Manual (Maas and Weiss, 2007). Active contraction was incorporated into the muscle material model, with the total stress in the solid mixture (σ) as the sum of the solid stress due to strain (σ^s) and the active contractile stress (σ^a):

$$\sigma = \sigma^s + \sigma^a \tag{1}$$

The active contractile stress was uniform across all the elements in each muscle. Parameters of the constitutive model are shown in **Table 1**. Boundary conditions of the model are based on the fifth Grand Challenge Competition in which the gait data and *in vivo* measured knee contact forces of a subject were provided (Fregly et al., 2012). The femur was constrained in all degrees of freedom. Based on the trajectories of markers in the gait data, angles of the hip, knee and ankle of the subject during normal speed walking were derived in Visual 3D (V6; C-Motion, USA) and then used as inputs for the rotation of joints in the musculoskeletal model. The ground reaction force was applied to the foot.

In order to solve the muscle redundancy issue, active contractile stresses of the muscles in the finite element musculoskeletal model were optimized until 1) the cost function (i.e. sum of muscle active contractile stresses cubed: $\sum_{i=1}^{n}(\sigma^a)^3$ (Adouni et al., 2012)) was minimized and 2) the resultant knee moment approached zero ($\leq 0.3 \, \text{N} \times \text{m}$). The optimization was based on the muscle active contractile stresses and the corresponding joint moments in the FE model. Analyses were conducted at 15 evenly distributed time instances of the stance phase of a gait, starting from heel-strike (0s, 0%) to toe-off (0.7s, 100%).

To enhance computational efficiency, the finite element model at each quasi-static time instance (e.g. at 0.5s) in the optimization process was simulated based on the model at the previous time instance (i.e. at 0.45s) in which the optimization criteria were achieved, rather than starting from the original state (i.e. at 0s). Finite

element modelling was performed in FEBio (V2.6.4; http://febio.org/febio). MATLAB (R2017a, Mathworks, MA) was adopted for the optimization (fmincon function) and automation procedures. Active contractile stresses and tensile stresses of the muscles and contact pressure of the muscle-muscle and muscle-bone interactions were analyzed. To assess the validity of the model, the total contact force of the knee predicted by the musculoskeletal model was compared to *in vivo* measurement data of the same subject.

Results

The time instants at heel-strike, weight-acceptance, mid-stance, push-off and toe-off between the model predictions and the experimental measurement were closely comparable (**Fig. 2**). Compared to the experimental measurement, the predicted joint force was 1% higher at weight-acceptance, 21% lower at mid-stance and 12% higher at push-off, with a mean absolute percentage error of 11%.

As shown in **Fig. 3**, the hamstrings were primarily activated during heel-strike, while the quadriceps played the major role afterwards until toe-off. The maximum active contractile stress occurred in the vastus lateralis at push-off. The tensile stresses were concentrated in the tendon regions in which the tissue was thinner than the muscle regions (**Fig. 4**). The maximum tensile stress occurred in the hamstrings at heel-strike, while the minimum tensile stress of the muscles occurred at mid-stance. The maximum tensile stress of the quadriceps occurred at toe-off. As illustrated in **Fig. 5**, the muscle-muscle and muscle-bone contacts were evident. The level of contact pressure was minimal compared to the tensile stresses of the muscles.

Discussion

In this study, a finite element musculoskeletal model with 3D muscles and the ability to predict muscle contractions was developed for the first time. This new model provided stresses and strains of muscles and contact mechanics of the muscle-muscle and muscle-bone interactions, thus allowing for more systematic biomechanical evaluation of the musculoskeletal system compared with previous musculoskeletal models with 1D line-segment muscles.

The muscle redundancy issue that hampers pervious 3D muscle models was addressed through the optimization approach. Therefore, prediction of active contractile stresses of 3D muscles was enabled. In the optimization process, the finite element model at each quasi-static time instance was simulated based on the model at the previous time instance, rather than starting from the original time instance. By doing so, computational efficiency was improved by approximately 105 (i.e. $\sum_{k=1}^{14} k$) times for a quasi-static simulation including 15 analysis instances.

In this study, optimization was performed directly to the finite element musculoskeletal model. Any region of the musculoskeletal model including muscles, joints, ligaments and bones can be set as 3D deformable contact models with ease. Due to the large number of degrees of freedom involved, the simulation was completed in approximately 5 days using a Windows 10 desktop with 32 GB of RAM and 16 Intel E5-2699 cores at 2.2 GHz. Further development of the model will focus on enhancing the computational efficiency though a hybrid model incorporating both 3D and 1D muscles once the muscles that can be simplified as 1D without compromising accuracy are targeted.

Generally, the knee contact force predicted by the computer model corresponded reasonably well to the *in vivo* measurement. The difference in comparison might be due to the model simplification described in the paragraph below and the musculoskeletal variations between the subjects of the two databases, apart from errors of the *in vivo* measurement. Although muscle contractions can be reflected by knee contact forces to some extent, active contractile stresses of individual muscles were not compared to the experimental data such as electromyography (EMG) signals due to uncertainties in acquisition and conversion of EMG signals into muscle contractions. Future imaging measurements might serve as alternative effective approaches to validate deformation of 3D muscle models during motion. The presence of contact and wrapping between muscles and surrounding tissues found in this study further demonstrated the need to consider 3D contact models of muscles, which is in agreement with the study of Webb et al. (2014).

The primary aim of this study was to develop the necessary modelling methodology for incorporating 3D muscles into musculoskeletal models with the redundancy issue of muscle contractions addressed. Whilst this was achieved, there were some limitations. First, strains in the muscles were assumed to be zero in the original model configuration. These data would be provided by future experiments measuring initial stretches within muscle fibres (Webb et al., 2014). Future experiments are also needed to offer more realistic data to define the regions of tendon and muscle tissues and orientation of fibres and non-uniform activation within muscles for these models. Constitutive models involving the relationship between muscle contraction and fibre stretch will be accounted for in future studies. Although the muscles considered in this model play the principal role in flexion and extension of the knee (Lieb and Perry, 1968, Fukunaga et al., 1992, Jenkins, 2008, Yeow, 2013, Lube et al., 2016), incorporation of the complete muscles in the lower extremity would further enhance the modelling accuracy. Contact joint models (Chen et al., 2015, Shu et al., 2018) will also be incorporated in future studies to enhance the modelling accuracy.

The finite element model was solved quasi-statically through an implicit solver ignoring the dynamic effect, because the implicit method is more reliable than the explicit method for dynamic analyses involving relatively low-speed activities owning to its iterative approach (Naghibi Beidokhti et al., 2016). Additionally, the quasi-static approach is more efficient, as simulations can be performed only at the time instances that are of interest rather than for the whole period. It should be noted that the optimization approach developed to solve the muscle redundancy issue can be also applied to explicit models, because both the simulation and optimization at each time instance were performed continuously based on the optimized results at the previous time instance. This modelling framework serves as the methodological basis for developing musculoskeletal

modelling systems in finite element method incorporating 3D deformable contact models of muscles, joints, ligaments and bones.

Acknowledgements

Conflict of interest

The authors declare no conflict of personal or financial interests.

References

ADOUNI, M., SHIRAZI-ADL, A. & SHIRAZI, R. 2012. Computational biodynamics of human knee joint in gait: From muscle forces to cartilage stresses. *Journal of Biomechanics,* 45**,** 2149-2156.

BLEMKER, S. S., PINSKY, P. M. & DELP, S. L. 2005. A 3D model of muscle reveals the causes of nonuniform strains in the biceps brachii. *Journal of Biomechanics,* 38**,** 657-665.

CARBONE, V., FLUIT, R., PELLIKAAN, P., VAN DER KROGT, M. M., JANSSEN, D., DAMSGAARD, M., VIGNERON, L., FEILKAS, T., KOOPMAN, H. F. J. M. & VERDONSCHOT, N. 2015. TLEM 2.0 – A comprehensive musculoskeletal geometry dataset for subject-specific modeling of lower extremity. *Journal of Biomechanics,* 48**,** 734-741.

CHEN, Z., WANG, L., LIU, Y., HE, J., LIAN, Q., LI, D. & JIN, Z. 2015. Effect of component mal-rotation on knee loading in total knee arthroplasty using multi-body dynamics modeling under a simulated walking gait. *Journal of Orthopaedic Research,* 33**,** 1287-1296.

DRAKE, R., VOGL, A. W. & MITCHELL, A. W. 2009. *Gray's Anatomy for Students E-Book*, Elsevier Health Sciences.

FREGLY, B. J., BESIER, T. F., LLOYD, D. G., DELP, S. L., BANKS, S. A., PANDY, M. G. & D'LIMA, D. D. 2012. Grand challenge competition to predict in vivo knee loads. *Journal of Orthopaedic Research,* 30**,** 503-513.

FUKUNAGA, T., ROY, R. R., SHELLOCK, F. G., HODGSON, J. A., DAY, M. K., LEE, P. L., KWONG-FU, H. & EDGERTON, V. R. 1992. Physiological cross-sectional area of human leg muscles based on magnetic resonance imaging. *Journal of Orthopaedic Research,* 10**,** 926-934.

HALLORAN, J. P., ACKERMANN, M., ERDEMIR, A. & VAN DEN BOGERT, A. J. 2010. Concurrent musculoskeletal dynamics and finite element analysis predicts altered gait patterns to reduce foot tissue loading. *Journal of Biomechanics,* 43**,** 2810-2815.

JENKINS, D. B. 2008. *Hollinshead's Functional Anatomy of the Limbs and Back-E-Book*, Elsevier Health Sciences.

LI, J., MCWILLIAMS, A. B., JIN, Z., FISHER, J., STONE, M. H., REDMOND, A. C. & STEWART, T. D. 2015. Unilateral total hip replacement patients with symptomatic leg length inequality have abnormal hip biomechanics during walking. *Clinical Biomechanics* 30**,** 513-519.

LIEB, F. J. & PERRY, J. 1968. Quadriceps Function: an anatomical and mechanical study using amputated limbs. *JBJS,* 50**,** 1535-1548.

LUBE, J., COTOFANA, S., BECHMANN, I., MILANI, T. L., ÖZKURTUL, O., SAKAI, T., STEINKE, H. & HAMMER, N. 2016. Reference data on muscle volumes of healthy human pelvis and lower extremity muscles: an in vivo magnetic resonance imaging feasibility study. *Surgical and Radiologic Anatomy,* 38**,** 97-106.

MAAS, S. A. & WEISS, J. A. 2007. *FEBio Theory Manual*, http://mrl.sci.utah.edu/software/febio.

MO, F., LI, F., BEHR, M., XIAO, Z., ZHANG, G. & DU, X. 2018. A lower limb-pelvis finite element model with 3D active muscles. *Annals of Biomedical Engineering,* 46**,** 86-96.

NAGHIBI BEIDOKHTI, H., JANSSEN, D., KHOSHGOFTAR, M., SPRENGERS, A., PERDAHCIOGLU, E. S., VAN DEN BOOGAARD, T. & VERDONSCHOT, N. 2016. A comparison between dynamic implicit and explicit finite element simulations of the native knee joint. *Medical Engineering & Physics,* 38**,** 1123-1130.

RÖHRLE, O. & PULLAN, A. J. 2007. Three-dimensional finite element modelling of muscle forces during mastication. *Journal of Biomechanics,* 40**,** 3363-3372.

SHU, L., YAMAMOTO, K., YAO, J., SARASWAT, P., LIU, Y., MITSUISHI, M. & SUGITA, N. 2018. A subject-specific finite element musculoskeletal framework for mechanics analysis of a total knee replacement. *Journal of Biomechanics,* 77**,** 146-154.

TERAN, J., SIFAKIS, E., BLEMKER, S. S., NG-THOW-HING, V., LAU, C. & FEDKIW, R. 2005. Creating and simulating skeletal muscle from the visible human data set. *IEEE Transactions on Visualization and Computer Graphics,* 11**,** 317-328.

WEBB, J. D., BLEMKER, S. S. & DELP, S. L. 2014. 3D finite element models of shoulder muscles for computing lines of actions and moment arms. *Computer Methods in Biomechanics and Biomedical Engineering,* 17**,** 829-837.

WEISS, J. A., MAKER, B. N. & GOVINDJEE, S. 1996. Finite element implementation of incompressible, transversely isotropic hyperelasticity. *Computer Methods in Applied Mechanics and Engineering,* 135**,** 107-128.

YEOW, C. H. 2013. Hamstrings and quadriceps muscle contributions to energy generation and dissipation at the knee joint during stance, swing and flight phases of level running. *The Knee,* 20**,** 100-105.

ZÖLLNER, A. M., POK, J. M., MCWALTER, E. J., GOLD, G. E. & KUHL, E. 2015. On high heels and short muscles: A multiscale model for sarcomere loss in the gastrocnemius muscle. *Journal of Theoretical Biology,* 365**,** 301-310.

Figures
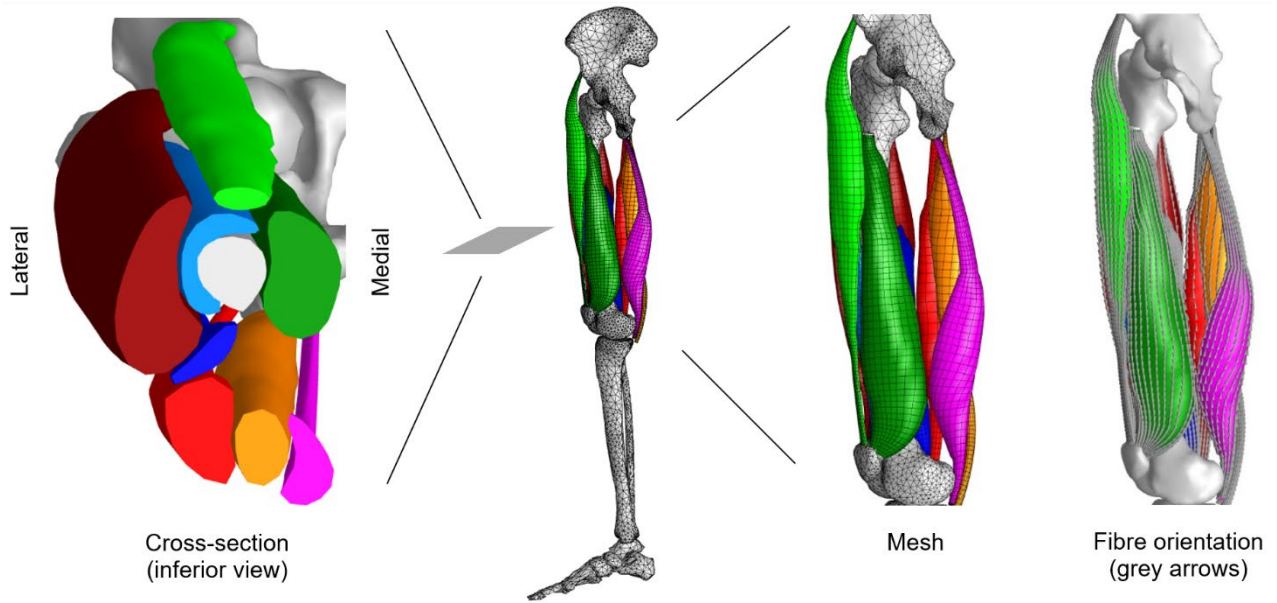
Fig. 1. The finite element musculoskeletal model with 3D muscles. Fibre orientation in the muscles was illustrated by the grey arrows. The principal muscles involved in flexion/extension of the knee were incorporated in the model, including rectus femoris (light green), vastus lateralis (dark red), vastus intermedius (light blue), vastus medialis (dark green), semitendinosus (orange), semimembranosus (pink), biceps femoris caput breve (dark blue) and biceps femoris caput longum (light red).
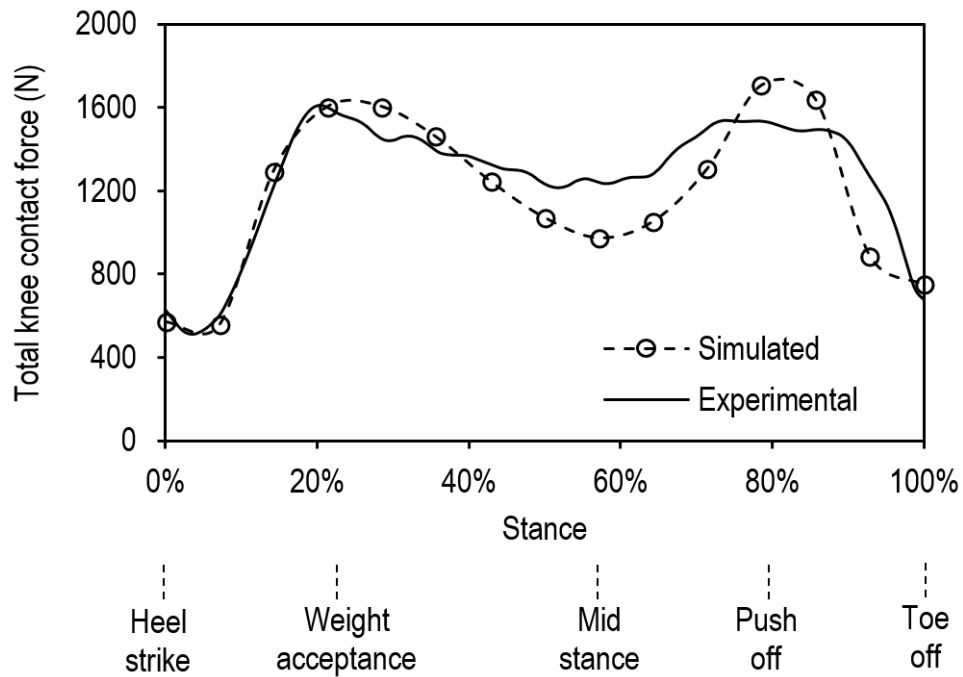
Fig. 2. Comparison of the predicted total contact forces of the knee and the *in vivo* measurement data. The time instants at heel-strike, weight-acceptance, mid-stance, push-off and toe-off between the model predictions and the experimental measurement were closely comparable. Compared to the experimental measurement, the predicted joint force was 1% higher at weight-acceptance, 21% lower at mid-stance and 12% higher at push-off, with a mean absolute percentage error of 11%. The 15 analyzed instances in the model were circle-marked.
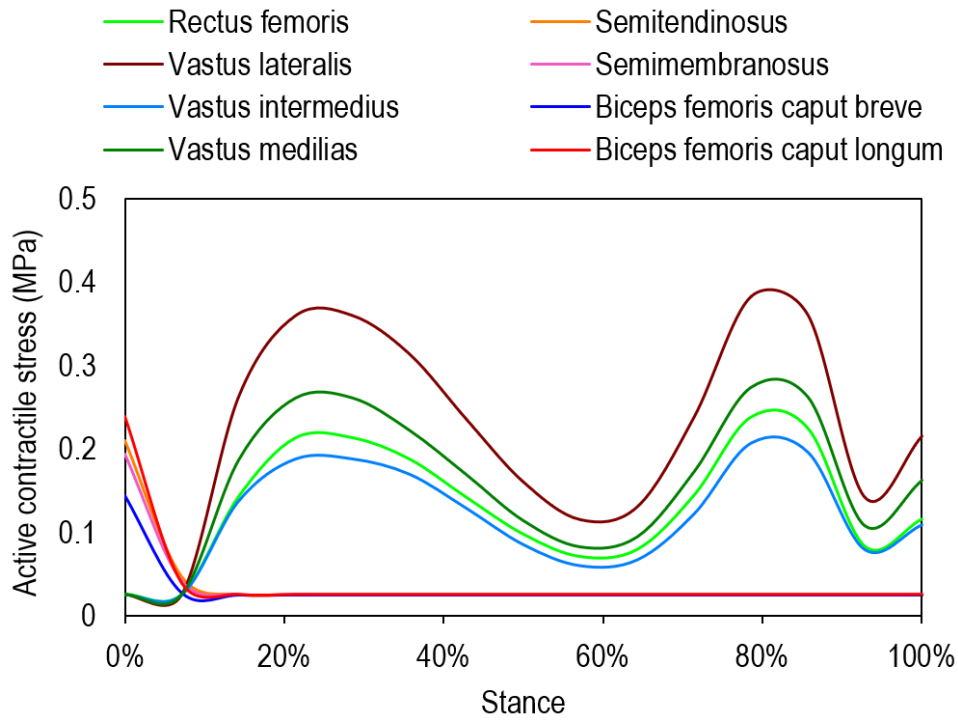
Fig. 3. Active contractile stresses of the muscles determined through optimization. The hamstrings were primarily activated during heel-strike, while the quadriceps played the major role afterwards until toe-off. Analyses were conducted at 15 evenly distributed time instances of the stance cycle.
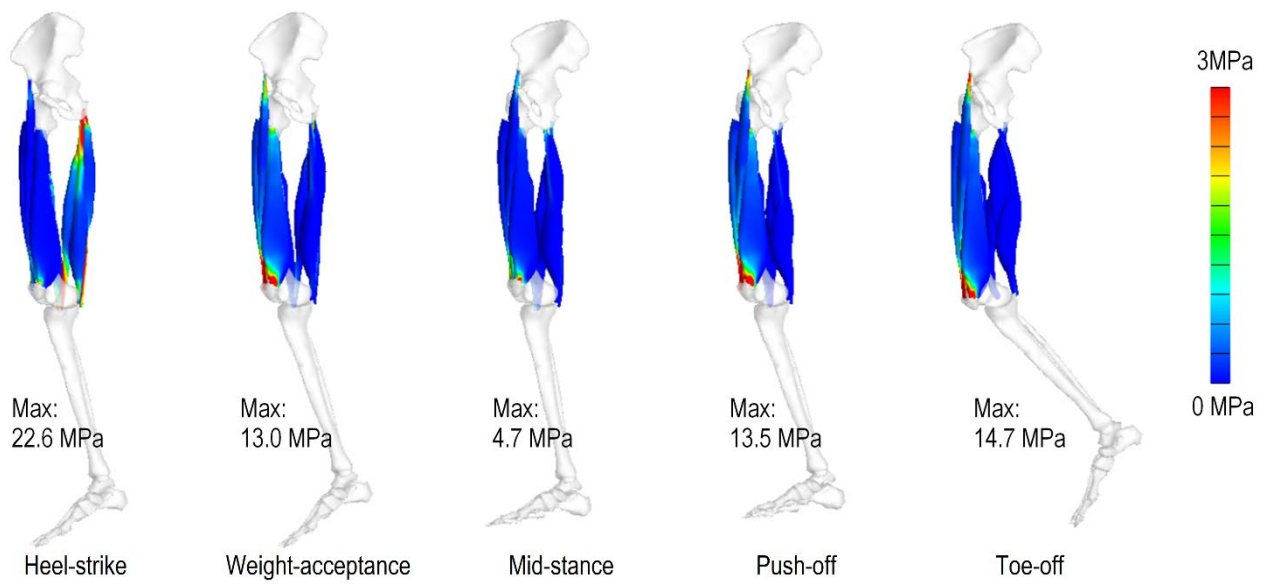
Fig. 4. Tensile stresses (MPa) in the muscles at the characteristic gait phases. Tensile stresses were concerntrated in the tendon regions connecting the bones. The maximum tensile stress occurred in the hamstrings at heel-strike, while the minimum tensile stress of the muscles occurred at mid-stance. The maximum tensile stress of the quadriceps was found at toe-off.
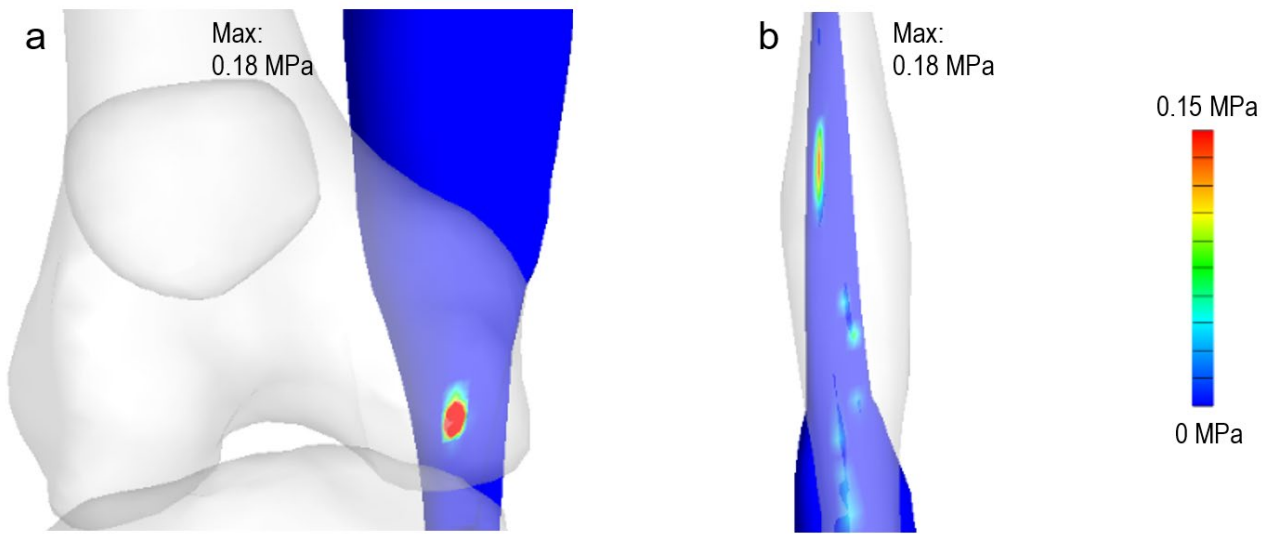
Fig. 5. Contact pressure (MPa) of the semimembranosus in contact with the distal femur (a; anterior view) and the semitendinosus (b; posterior view) at heel-strike, as an example to illustrate contact mechanics of the muscle-muscle and muscle-bone interactions.

List of Tables

Table 1. Constitutive model parameters. The values were based on previous studies (Blemker et al., 2005, Teran et al., 2005, Röhrle and Pullan, 2007, Mo et al., 2018). These parameters were described in detail in sections 5.3.1 and 5.3.5 of the FEBio Theory Manual (V2.6) (Maas and Weiss, 2007). σ^{a}_{min} and σ^{a}_{max} are the minimum and maximum values of the active contractile stress (σ^{a}) respectively used in the optimization procedure.

Muscle constants		Tendon constants	
C_1	0.01 MPa	C_1	0.1 MPa
C_2	0.01 MPa	C_2	0.1 MPa
C_3	0.015 MPa	C_3	2.7 MPa
C_4	15	C_4	46.4
C_5	6 MPa	C_5	500 MPa
K	10 MPa	K	100 MPa
λ_m	1.4	λ_m	1.03
σ^{a}_{min}	0.025 MPa		
σ^{a}_{max}	0.5 MPa		